

## Epitaxial growth of the heavy-fermion $\text{UCu}_5$ (111) film on the Cu (111) substrate and its electronic structure study

Wei Feng <sup>\*,†</sup>, Qunqing Hao <sup>\*</sup>, Xiangfei Yang, Qiang Zhang, Jian Wu, Qin Liu , Yun Zhang, Shiyong Tan, Qiuyun Chen <sup>‡</sup> and Xinchun Lai

*Science and Technology on Surface Physics and Chemistry Laboratory, Mianyang 621908, China*



(Received 4 March 2024; accepted 11 June 2024; published 2 July 2024)

Uranium-based compounds display rich and exotic physical properties, but remain less studied compared with  $4f$ -electron rare-earth compounds. The lack of high quality single crystal samples hinders the use of many specific techniques to study the properties of uranium-based compounds. In the present study, we successfully obtain high quality single crystalline  $\text{UCu}_5$  (111) films by depositing uranium atoms on the Cu (111) substrate after annealing at 800 K. Surface structures with the increase of uranium coverage have been systematically studied, and moiré patterns are observed in the  $\text{UCu}_5$  (111) films, which gradually become weaker with the increase of film thickness of  $\text{UCu}_5$ .  $dI/dV$  spectra of  $\text{UCu}_5$  films with the thickness from 1 to 5 unit cells show similar electronic properties, which exhibit a strong asymmetric dip-peak structure near the Fermi energy. Temperature-dependent  $dI/dV$  measurements further confirm that this asymmetric feature is related to Kondo physics and due to the hybridization between U  $5f$  electrons and surrounding conduction electrons. Different terminated surfaces can be obtained by sputtering  $\text{UCu}_5$  thick films with  $\text{Ar}^+$  ions and subsequent annealing, which show drastically different electronic structure. Our results provide a path for the preparation of single crystalline uranium-based compounds and related materials.

DOI: [10.1103/PhysRevMaterials.8.074402](https://doi.org/10.1103/PhysRevMaterials.8.074402)

### I. INTRODUCTION

In condensed matter systems, intricate interactions between different degrees of freedom, such as charge, spin, and orbit, may give rise to diverse ground states, including unconventional superconductivity, magnetic order, non-Fermi liquid states, and intriguing charge and orbital order [1–5]. These ground states can be readily tuned by the external parameters, e.g., temperature, pressure, chemical doping or magnetic fields. Among the existing strongly correlated materials, heavy-fermion compounds containing  $4f$  or  $5f$  electrons exhibit the strongest electron correlation effects [3,6,7]. While most attention has been directed to the  $4f$ -electron-based rare-earth compounds, the actinide-based compounds remain less studied, although with richer physics. With partially filled  $5f$  shell electrons coupled with spin-orbit interaction, along with crystal field effects, phonons, magnons, and electron correlations at comparable energy scales, intricate physical properties appear in the uranium-based heavy-fermion compounds [8–11].

As a typical uranium-based heavy-fermion material,  $\text{UCu}_5$  undergoes a conventional antiferromagnetic transition with the Néel temperature of  $T_N \approx 15$  K, which was confirmed by magnetic susceptibility measurements [12–14]. With lowering temperature, an additional transition appears at  $T_2 \approx 1$  K, which was first found by Ott *et al.* [15]. The magnetic U

ions of  $\text{UCu}_5$  sit on a face-centered-cubic (fcc) lattice and form a network of edge-sharing tetrahedra—a geometry conducive to magnetic frustration. Powder neutron diffraction experiments definitely indicate that the antiferromagnetic order in both phases consists of localized U  $5f$ -electron spins pointing along the crystal unit cell's  $\langle 111 \rangle$  direction with ordering wave vectors' symmetry related to  $q = \langle 1/2, 1/2, 1/2 \rangle$  [13,16,17]. When the temperature decreases through  $T_2$ , the magnitude of  $q$  does not change despite there being clear signs of a phase transition in the magnetization, resistivity, and specific heat data [15,18]. The simplest magnetic order consistent with these data is the  $1-q$  configuration, where the spins ferromagnetically aligned within the (111) planes, but antiferromagnetically aligned with the neighboring (111) planes [13]. Another magnetic order—a quadruple- $q$  structure ( $4-q$ ) was firstly proposed by Nakamura, which is consistent not only with the previous powder neutron diffraction experiments but also with the nuclear magnetic resonance (NMR) experiments [19]. Due to the lack of single crystals of  $\text{UCu}_5$ , it is impossible to distinguish a multidomain  $1-q$  configuration from the more complex  $4-q$  variants experimentally using powder neutron diffraction measurements. Therefore, whether  $\text{UCu}_5$  first enters  $4-q$  or  $1-q$  below 15 K has remained controversial for a long time. Although there are many indirect experimental results supporting that  $\text{UCu}_5$  first transforms into the  $4-q$  structure at 15 K, and then into the  $1-q$  configuration below 1 K [18–23], Hall effect studies on polycrystalline  $\text{UCu}_5$  indicate that the magnetic order between 15 and 1 K is the  $1-q$  configuration [24], which is completely contrary to the previous results. In addition, some researchers found absorption in the far infrared below 15 K from the optical

\*These authors contributed equally to this work.

†Contact author: fengwei610@163.com

‡Contact author: sheqiyun@126.com

experiments, which was ascribed to the excitations across a spin-density-wave (SDW) type gap and indicates the itinerant nature of the magnetic phase transition [25–27]. It is another puzzle whether this is a SDW type gap or the commensurate magnetic order. Experimental results on the electronic structure of  $\text{UCu}_5$  were obtained relatively early, in the 1980s [28,29]; they are based on the core level and valence band analysis on the polycrystalline samples without angle resolved information, and there is little research on the evolution of the electronic structure before and after this phase transition. Due to the difficulty in preparing bulk single crystals, an innovative way to resolve the above controversy about the magnetic structures during this phase transition is to prepare single crystal thin films.

In the present work,  $\text{UCu}_5$  single crystal films have been prepared by depositing U atoms onto the Cu (111) substrate after annealing at 800 K in ultrahigh vacuum conditions. Scanning tunneling microscopy (STM) and low energy electron diffraction (LEED) measurements have been used to confirm the surface structure. When uranium atoms are deposited onto the Cu (111) substrate after annealing at 800 K, a wetting layer will first form and then  $\text{UCu}_5$  (111) films with moiré patterns grow. The moiré patterns gradually decrease with the increase of film thickness and finally disappear in the 5 UC film.  $dI/dV$  spectra show similar electronic properties of  $\text{UCu}_5$  films with different thickness. Temperature-dependent  $dI/dV$  spectra on the 11 unit cell (u.c.) film show that the asymmetric structure near the Fermi energy originates from the Kondo physics. Different terminated surfaces with various electronic properties can be obtained by sputtering  $\text{UCu}_5$  thin films with  $\text{Ar}^+$  ions and subsequent annealing. Our work provides a method in the preparation of single crystalline uranium-based compounds, which is important for the future study of the magnetic structure of  $\text{UCu}_5$ .

## II. RESULTS

$\text{UCu}_5$  crystallizes in a face-centered-cubic structure of the  $F-43m$  space group with the lattice constant of 7.033 Å, as shown in Fig. 1(a). Along the  $\langle 111 \rangle$  direction, each unit cell is composed of four atomic layers, including three layers of copper atoms and one layer of uranium atoms. Among them, the interlayer spacing between two layers of copper atoms is relatively small, and when they are stacked together, a honeycomb structure is formed, which can be clearly observed in Fig. 1(d). Meanwhile, another layer of copper atoms forms a kagome structure and uranium atoms form a triangular structure, as shown in Fig. 1(c). The stacking relationship between them can be seen from the side and top views in Figs. 1(b) and 1(c), and the red, yellow, and blue spheres represent the honeycomb, kagome copper atoms, and U atoms, respectively. The in-plane lattice constant of  $\text{UCu}_5$  (111) is 4.97 Å, which is twice the in-plane lattice constant of the Cu (111) surface and the mismatch is about 2.5%, so the Cu (111) surface can not only serve as an excellent substrate for the epitaxial growth of  $\text{UCu}_5$  (111) thin films, but also provide a source of copper atoms for the preparing of  $\text{UCu}_5$ . In addition, according to the phase diagram of the U-Cu binary alloy [30],  $\text{UCu}_5$  is the only product after the reaction of U and Cu elements, which can

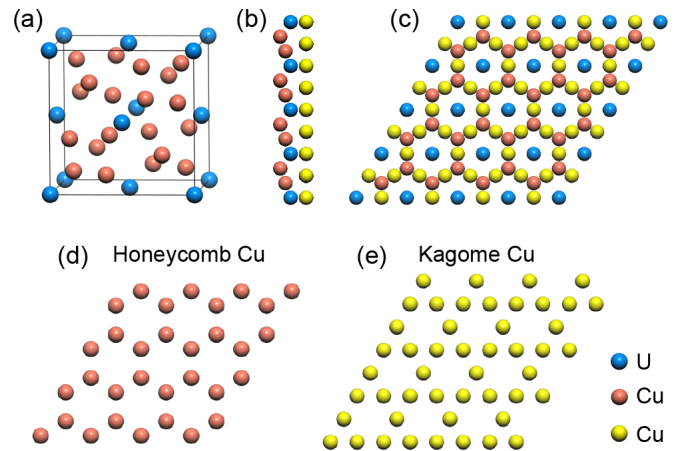


FIG. 1. Crystal structure and composition information of  $\text{UCu}_5$ . (a) Crystal structure of  $\text{UCu}_5$ . (b) Side and (c) top views of one unit cell of  $\text{UCu}_5$  (111). The red, yellow, and blue spheres represent honeycomb, kagome copper atoms, and uranium atoms, respectively. (d), (e) Atomic arrangement of the honeycomb Cu (d) and kagome Cu (e) layers in  $\text{UCu}_5$ .

avoid the interference of other compounds during preparation and obtain a completely pure  $\text{UCu}_5$  phase.

In a previous study [31], we have explored the adsorptions, reactions, and electronic properties of individual uranium atoms on Cu (111) and found that upon deposition of a small amount of uranium onto Cu (111) at 8 K, individual uranium atoms show relatively high activity and react with the Cu (111) surface at low temperature. Here the substrate is kept at room or much higher temperature. Figure 2 displays the growth process of the epitaxial  $\text{UCu}_5$  film as the coverage gradually increases. When a small amount of uranium atoms is deposited onto the surface at room temperature, uranium atoms mainly aggregate at the edge of the steps or form irregular islands on the terraces, as shown in Fig. 2(b). The growth rate can also be determined from the coverage by depositing a small amount of U atoms on Cu (111), which is about 1 u.c./h. After annealing at 800 K for about 5 min, all of these irregular islands become atomically smooth nanostructures, and the remaining part of the surface is still bare Cu (111) [Fig. 2(c)]. The observed nanostructure is the first layer formed on the Cu (111) surface and is the interface between  $\text{UCu}_5$  (111) and the Cu (111) substrate with unique features (which will be discussed later), and here we name it the “wetting layer.” When the deposited uranium atoms reach about a half layer, new nanostructures with typical long period moiré patterns appear on the annealed sample in addition to the wetting layer [Fig. 2(d)]. There are also some bright spots on the surface, which are mainly unordered irregular U islands that remain on the surface, and their height can be found from the height profiles in Figs. 2(g)–2(i). The newly formed nanostructure with moiré patterns is mainly the  $\text{UCu}_5$  film, which subsequently grows on the wetting layer; its thickness can be defined in units of the unit cell (u.c.). When the substrate is kept at the much higher temperature of 800 K, a thicker  $\text{UCu}_5$  film can be obtained by directly depositing uranium atoms onto the surface. As can be seen in Fig. 2(e), most of the sample surface exhibits long period moiré patterns of the  $\text{UCu}_5$  film, while the

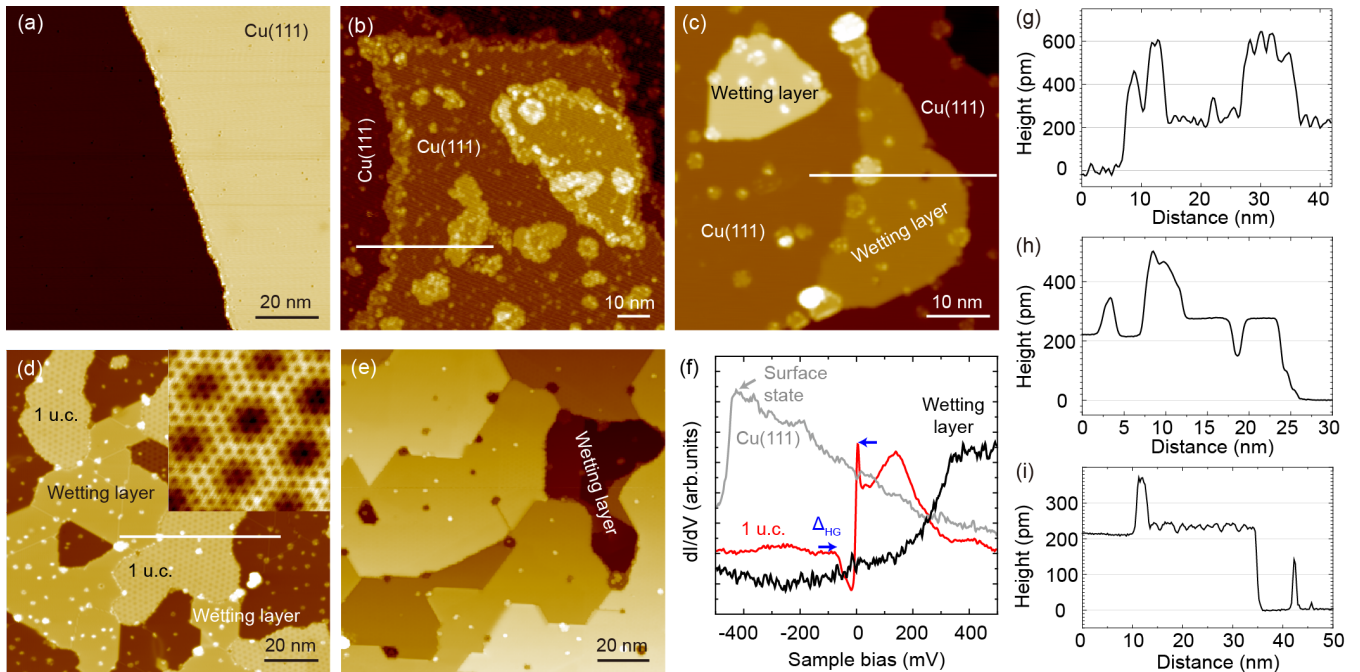


FIG. 2. Growth process of the epitaxial  $\text{UCu}_5$  (111) thin film. (a) Surface morphology of the Cu (111) substrate. (b), (c) Sample morphology of the substrate after depositing a very small amount of uranium atoms onto the surface at room temperature (b), as well as after annealing at 800 K for 5 min (c). (d) Sample morphology of the substrate after depositing 0.5 ML of uranium atoms onto the surface after annealing at 800 K for 5 min. The inset shows the atomic resolution image of the moiré pattern on the 1 u.c. regions. (e) Sample morphology of the  $\text{UCu}_5$  (111) film with nominal thickness increased to 3.5 u.c.; the film was obtained by directly evaporating more uranium atoms onto the substrate at 800 K. (f)  $dI/dV$  spectra obtained on the Cu (111) substrate, wetting layer, and 1 u.c.  $\text{UCu}_5$  film at 4.8 K. (g)–(i) Height profiles correspond to the white lines in (b), (c), (d), respectively. (a)  $V_s = 1.0$  V,  $I_t = 300$  pA. (b)  $V_s = 1.0$  V,  $I_t = 200$  pA. (c)  $V_s = 1.0$  V,  $I_t = 200$  pA. (d)  $V_s = 0.1$  V,  $I_t = 300$  pA. Inset of (d)  $V_s = 0.003$  V,  $I_t = 3.2$  nA. (e)  $V_s = 0.35$  V,  $I_t = 200$  pA.

wetting layers can only be observed in a small region. These surfaces can also be identified from the drastically different  $dI/dV$  spectra. As can be seen in Fig. 2(f), the surface state of Cu (111) can be apparently observed at  $-0.4$  V, and for the wetting layer there is a clearly empty state at 0.35 V, while the empty state of the  $\text{UCu}_5$  thin film shifts to 0.15 V. What stands out in the spectra is that the wetting layer does not show any obvious state near the Fermi energy, while a strong asymmetric dip-peak structure near the Fermi energy can be clearly observed on the surfaces of the  $\text{UCu}_5$  film. Details of this asymmetric structure will be discussed later. It is noteworthy that  $\text{UCu}_5$  orders magnetically below 15 K, and our measuring temperature is about 4.8 K, which creates a bit of concern as to whether our sample shows any sign of being magnetically below 15 K. We have conducted a systematic study of this question, and indeed confirmed that the magnetic transition occurs in our films. We also studied the relationship between the film thickness and the transition temperature, and found that the magnetic transition temperature decreases with film thickness. These results will appear in a forthcoming paper.

To gain more insight on the atomic structure of the wetting layer and the  $\text{UCu}_5$  film, the atomic resolution images and LEED patterns of the Cu (111) substrate, the wetting layer, and the epitaxial  $\text{UCu}_5$  (111) film with different thickness are studied (Fig. 3). All the surfaces exhibit honeycomb structures, so the terminated surface of the naturally grown

$\text{UCu}_5$  (111) film can be recognized as the honeycomb Cu in Fig. 1(d). Furthermore, for the epitaxially grown  $\text{UCu}_5$  (111) film, all the surface copper atoms have been relaxed to the same height. Meanwhile, U atoms in the next layer locate at the center of the honeycomb structure. Comparing the distribution of uranium atoms in the wetting layer with the  $\text{UCu}_5$  (111) film, we found that the arrangement direction of uranium atoms in the wetting layer is consistent with that of the Cu (111) substrate, while it rotates  $30^\circ$  in the  $\text{UCu}_5$  (111) film compared with that of the Cu (111) surface. This angular relationship can also be clearly seen in the LEED patterns in Figs. 3(b)–3(h). The LEED patterns of the wetting layer in Fig. 3(d) display the same orientation as that of the Cu (111) substrate in Fig. 3(b), while newly weak LEED patterns start to appear in the 1 u.c.  $\text{UCu}_5$  (111) film and become obvious in the thicker  $\text{UCu}_5$  (111) film. The orientation of the LEED patterns of the  $\text{UCu}_5$  (111) film rotates  $30^\circ$  relative to the Cu (111) substrate, which is consistent with the atomic resolution images from the STM data in Fig. 3.

The evaporated uranium atoms first react with the surface copper atoms to form a wetting layer; then the reactive diffusion between uranium atoms and copper atoms during annealing promotes the forming of the thick film above the wetting layer. In some regions of the sample in Fig. 2(d), we found that before the wetting layer reaches full coverage, a 1 u.c. thick  $\text{UCu}_5$  (111) film with moiré patterns also appears on the sample surface, which can also be found in Fig. 4(a).

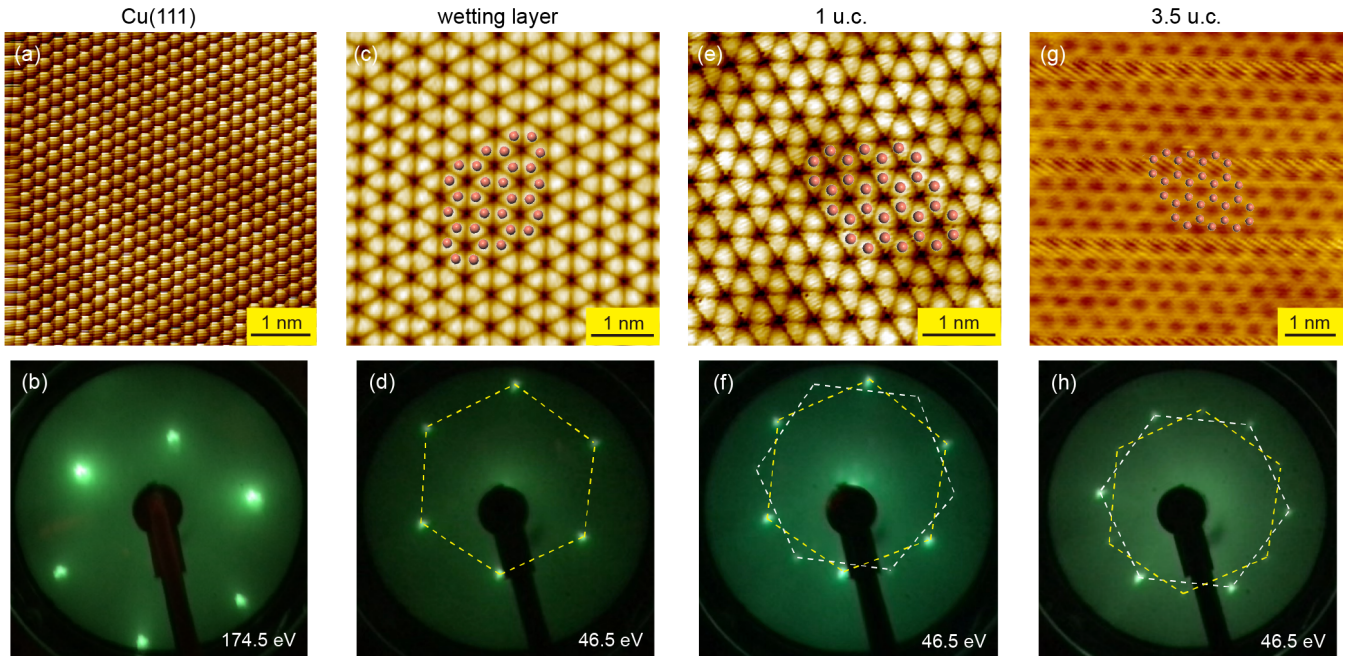


FIG. 3. Atomic resolution images and relative LEED patterns of the Cu (111) substrate and epitaxial UCu<sub>5</sub> (111) thin film as the coverage gradually increases. (a), (b) Cu (111) substrate. (c), (d) The wetting layer grown on the substrate before the formation of UCu<sub>5</sub> (111) thin film. (e), (f) The first UC of UCu<sub>5</sub> (111) thin film with moiré pattern beginning to grow on the wetting layer. (g), (h) UCu<sub>5</sub> (111) thin film with nominal thickness increased to 3.5 u.c. (a)  $V_s = -0.01$  V,  $I_t = 203.5$  nA. (c)  $V_s = -0.002$  V,  $I_t = 59.5$  nA. (e)  $V_s = -0.002$  V,  $I_t = 45$  nA. (g)  $V_s = 0.003$  V,  $I_t = 10.1$  nA.

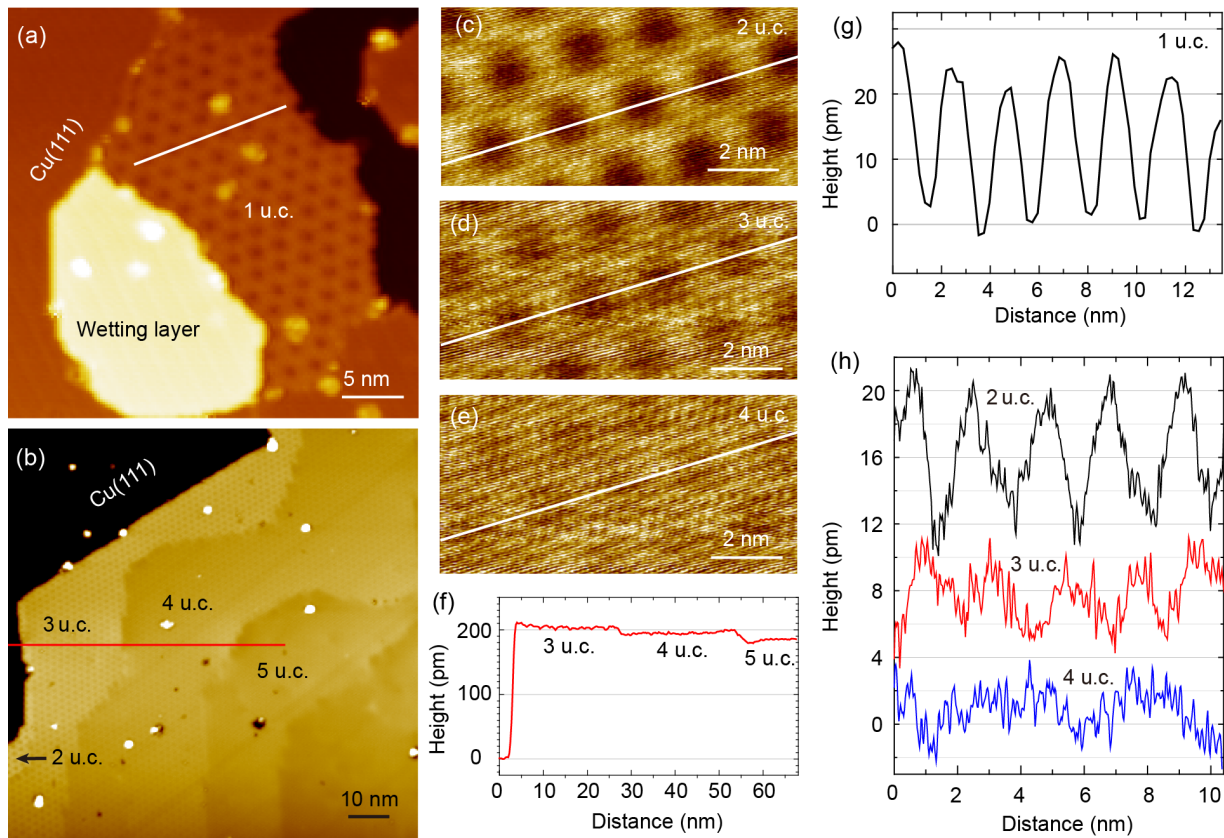


FIG. 4. (a), (b) STM images of the substrates and UCu<sub>5</sub> (111) films with different thicknesses, obtained at 78 K,  $V_s = 0.25$  V,  $I_t = 200$  pA. (c)–(e) Enlarged STM images of the moiré patterns with different thicknesses. (f) The height profile corresponding to the red line in (b). (g), (h) The height profiles of the moiré patterns obtained at the white solid lines marked in (a), (c)–(e).

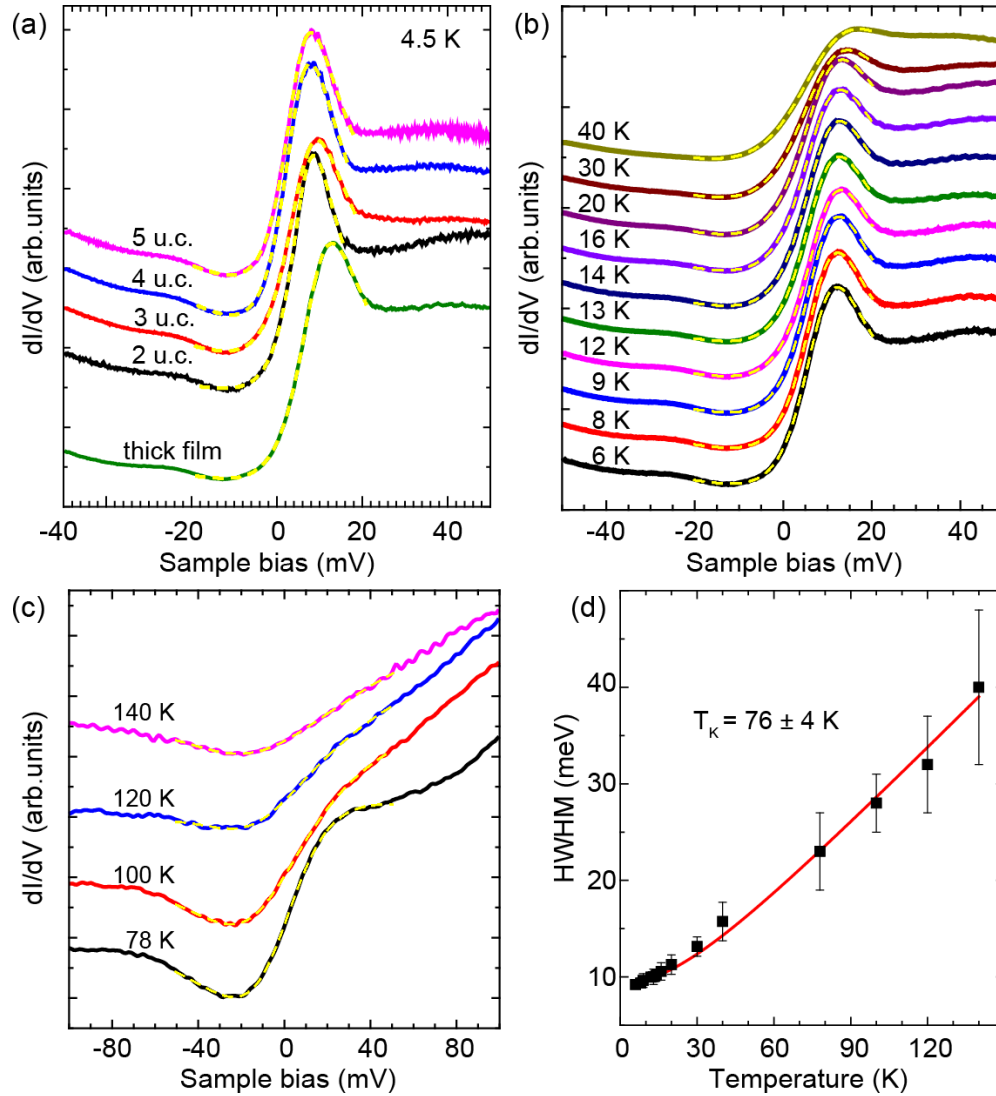


FIG. 5. (a)  $dI/dV$  spectra obtained on the surfaces of  $\text{UCu}_5$  (111) films with different thicknesses. (b), (c) Temperature evolution of the  $dI/dV$  spectra of the  $\text{UCu}_5$  (111) film with nominal thickness of about 11 u.c.; yellow dashed lines show the Fano fit of the  $dI/dV$  spectra. (d) Temperature dependence of HWHM of the peak near the Fermi level; the red curve represents temperature dependence of the width for a single Kondo impurity model.

If we deposit nearly 1 monolayer (ML) of uranium atoms on the Cu (111) surface at 800 K,  $\text{UCu}_5$  films with different thicknesses on the same sample can be obtained, as presented in Fig. 4(b). When the  $dI/dV$  spectra measurements were performed on this sample, we found that  $\text{UCu}_5$  films with the thickness from 1 to 5 u.c. possess similar electronic states, as shown in Fig. 5(a). All the spectra of  $\text{UCu}_5$  films with different thicknesses exhibit a strong asymmetric dip-peak structure near the Fermi energy. This asymmetric structure fully conforms to the hybridization gap of the heavy-fermion materials ( $\Delta_{\text{HG}}$ ) [32,33], and the gap size is approximately 70 mV with the peak positions locating at about 10 and  $-60$  mV, as shown in Fig. 2(f).

It is worth noting that the moiré patterns in the thicker  $\text{UCu}_5$  (111) film are much weaker than that in the 1 u.c. film. Figures 4(c)–4(e) display the moiré patterns with different thicknesses, and it is obvious that with the increase of film thickness, the moiré patterns gradually become weaker; no

moiré patterns can be observed on the surface of the 5 u.c. thick film. From the line profile in Fig. 4(g), the apparent height of the moiré patterns on the 1 u.c.  $\text{UCu}_5$  film is nearly 20 pm, and it decreases to about 8 pm in the 2 u.c.  $\text{UCu}_5$  film, which becomes about 4 pm in the 3 u.c.  $\text{UCu}_5$  film and totally disappears in the 5 u.c.  $\text{UCu}_5$  film. Comparing the height of the moiré patterns on the films with various thicknesses in Figs. 4(g) and 4(h), it can be concluded that the height of the moiré patterns decreases by half when the film thickness increases by 1 u.c. The appearance of moiré patterns is brought about by the rotation of the  $\text{UCu}_5$  film with respect to the Cu (111) substrate. From the orientation of LEED patterns presented in Fig. 3, the arrangement direction of uranium atoms in the wetting layer is consistent with that of the Cu (111) substrate, while it rotates  $30^\circ$  in the  $\text{UCu}_5$  (111) film compared with the Cu (111) surface. Due to the  $30^\circ$  rotation of the first  $\text{UCu}_5$  layer on top of the wetting layer, moiré patterns appear. With the increase of film thickness,

the following layers are not rotated and hence moiré patterns gradually become weak in the 2, 3, and 4 u.c.  $\text{UCu}_5$  films and finally disappear in the 5 u.c.  $\text{UCu}_5$  film.

In the  $dI/dV$  spectra measurements, we have found that  $\text{UCu}_5$  films with thicknesses from 1 to 5 u.c. possess similar electronic states, which exhibit a strong asymmetric dip-peak structure near the Fermi energy. To reveal the origin of this structure, temperature-dependent  $dI/dV$  measurements are carried out on the 11 u.c.  $\text{UCu}_5$  film, as shown in Figs. 5(b) and 5(c). With the increase of temperature, this asymmetric dip-peak structure becomes broadened, but a Fano line shape can still be observed at 140 K. This feature is similar to that of the Kondo resonance peak observed in many uranium-based compounds, like  $\text{USb}_2$  [32] and  $\text{URu}_2\text{Si}_2$  [34]. Considering that  $\text{UCu}_5$  is a typical heavy-fermion material, this peak is probably the Kondo coherent peak. In a Kondo system, the Fano line shape naturally occurs because of the presence of two interfering tunneling paths from the STM tip, one directly into the conduction electrons, and the other indirectly through the heavy quasiparticles. The Fano resonance has the following function form:

$$dI/dV \propto \frac{(\varepsilon + q)^2}{1 + \varepsilon^2}, \quad \varepsilon = \frac{eV - \varepsilon_0}{\Gamma}. \quad (1)$$

Here  $q$  reflects the quality of the ratio of probabilities between the two tunneling paths,  $\varepsilon_0$  is the energy location of the resonance, and  $\Gamma$  is the resonance half width at half maximum (HWHM) [34]. After fitting the  $dI/dV$  spectra in Fig. 5(a) with the Fano line shape (marked with yellow dashed lines), we found that the fitting curves were consistent with the experimental data ( $q = 2.3 \pm 0.4$ ,  $\Gamma = 8.5 \pm 0.5$ ). In addition, a temperature-dependent STS analysis was carried out on the thick film, as shown in Figs. 5(b) and 5(c). It was found that the resonance peak became weaker and wider with the increasing of temperature until 140 K. The corresponding HWHMs can be obtained by Fano fitting of the  $dI/dV$  curves at different temperatures, as shown in Fig. 5(d). It is clear that the HWHMs of the peak increase with the increasing of temperature. A single channel spin one-half Kondo impurity model in a Fermi-liquid regime has been used to describe the temperature dependence of HWHM as follows:

$$\text{HWHM} = \sqrt{(\pi k_B T)^2 + 2(k_B T_K)^2}. \quad (2)$$

From this equation, the obtained Kondo temperature is  $76 \pm 4$  K. The success of this model in describing the behavior of the peak further indicates that it is related to Kondo physics and results from the hybridization of U  $5f$  electrons and surrounding conduction electrons.

In bulk  $\text{UCu}_5$ , there are three different terminated surfaces, while in our study of thin  $\text{UCu}_5$  (111) films (less than 20 u.c.), the exposed surface is mainly the honeycomb Cu surface, and the other two terminations cannot be naturally grown. So we prepared a thick  $\text{UCu}_5$  film (about 20 nm), and sputtered it using  $\text{Ar}^+$  ions with an energy of 1.0 kV and then annealed to 800 K; after this process two new surfaces with different characteristics appeared on the sample surface besides the honeycomb Cu-terminated surface, marked with A and B, respectively [Fig. 6(a)]. This gives us the opportunity to study the electronic properties of different

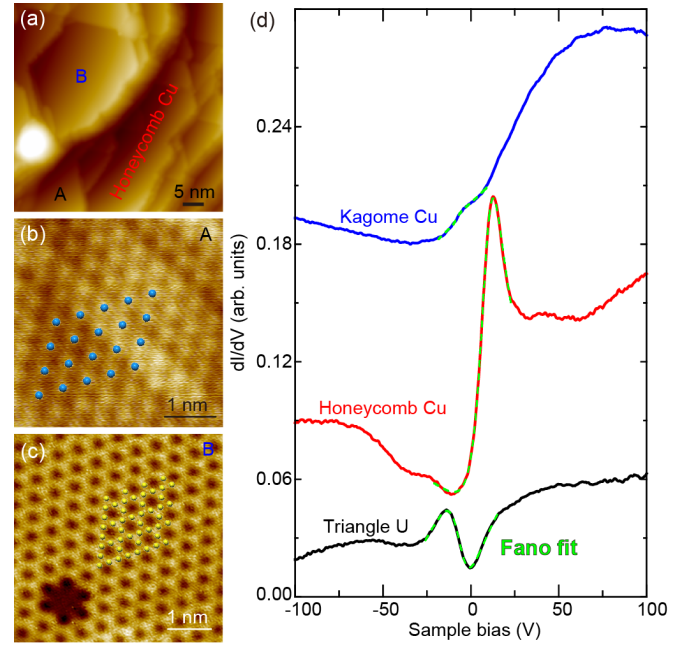


FIG. 6. (a) STM image of the  $\text{UCu}_5$  (111) thick film after sputtering and annealing treatment. In addition to the honeycomb Cu-terminated surface, two new terminated surfaces A and B appear;  $V_s = 0.4$  V,  $I_t = 200$  pA. (b) Atomically resolved STM image of surface A obtained at  $V_s = 0.006$  V,  $I_t = 35$  nA. (c) Atomically resolved STM image of surface B;  $V_s = 1.0$  V,  $I_t = 1.1$  nA. (d) The  $dI/dV$  spectra obtained on the three different terminated surfaces; significant hybridization gaps ( $\Delta_{\text{HG}}$ ) can be observed on the honeycomb Cu layer and triangle U layer (surface A).

terminations. Figures 6(b) and 6(c) provide the atomically resolved STM images of surfaces A and B, and different atomic arrangements can be observed for the two surfaces. The atomic arrangement and spacing of surface A is consistent with that of the U-terminated surface, and surface B is the kagome Cu surface.  $dI/dV$  spectra of these three different terminated surfaces differ significantly, as shown in Fig. 6(d), which can be used as a quick way to distinguish different terminated surfaces.  $dI/dV$  spectra of the three terminated surfaces exhibit similar features near the Fermi energy, which all display an asymmetric dip-peak structure. The difference is that the resonance's intensity near the Fermi energy taken on the A- and B-terminated surfaces is weaker than that on the honeycomb Cu-terminated surface. The observed asymmetric dip-peak spectrum feature resembles the well-studied Kondo resonance in many  $4f$  or  $5f$  systems, such as  $\text{CeCoIn}_5$  [33],  $\text{YbRh}_2\text{Si}_2$  [35],  $\text{USb}_2$  [32], and  $\text{URu}_2\text{Si}_2$  [36,37], which can be attributed to the interaction between the localized  $f$  electrons and conduction electrons. The spectra of two surfaces can be well fitted by the Fano equation, as shown in Fig. 6(d) by the green dashed lines. The Fano fits yield  $|q| = 2.43$ ,  $\varepsilon_0 = 10$  mV, and  $\Gamma = 8.8$  mV for the honeycomb Cu-terminated surface and  $|q| = 0.7$ ,  $\varepsilon_0 = -6$  mV, and  $\Gamma = 8.8$  mV for the U-terminated surface, respectively. For the kagome Cu surface, because the localized  $5f$  states at  $\sim 70$  mV are too close to the Fermi energy, the Fano line shape resonance falls on its shoulder and shows a small bump structure. Furthermore, its resonance intensity is the weakest among the three different

terminated surfaces, which makes the fitting procedure hard to reach. It should be noted that the Fano fits on the honeycomb Cu surface yield much larger  $q$  values than that obtained on the U-terminated surface. The value of  $q$  determines the line shape of the spectrum and generally produces a Lorentzian peak, a Lorentzian dip, and an asymmetric line shape as  $q$ , respectively, approaches infinity, 0, and 1, which essentially reflects the relative strength between indirect tunneling into the Kondo resonance state and direct tunneling into the itinerant states [38–41]. Here the  $|q|$  values of the resonances on the two terminated surfaces are both close to 1, which makes the spectrum feature exhibit an asymmetric structure with a peak and a dip. The much larger  $|q|$  values on the honeycomb Cu surface imply that electrons more readily tunnel into the Kondo-screened U-5*f* electrons instead of the itinerant conduction electrons.

In summary, single crystalline UCu<sub>5</sub> (111) films have been successfully obtained by depositing uranium atoms on the Cu (111) substrate after annealing at 800 K. When a small amount of uranium atoms is deposited onto the surface at room temperature, a wetting layer with drastically different electronic states from the substrate can be observed. With the increase of U coverage, new structures with typical long period moiré patterns appear on the surface, which arise from the rotation of the UCu<sub>5</sub> film to the wetting layer. The moiré patterns gradually become weaker with the increase of the film thickness of UCu<sub>5</sub> and disappear on the surface of the 5 u.c. thick UCu<sub>5</sub> film. By comparing the height of the moiré patterns of the films with various thicknesses, it can be observed that the height of the moiré patterns decreases by half when the film thickness increases by 1 u.c. Nevertheless, their electronic states remain similar and exhibit a strong asymmetric dip-peak structure near the Fermi energy, which is the indication of the Kondo resonance observed in 4*f* and 5*f* heavy-fermion compounds. Different terminated surfaces can

be obtained by sputtering thick UCu<sub>5</sub> films with Ar<sup>+</sup> ions and subsequent annealing, and their electronic structure shows a different character. Our results shed light on the preparation of single crystalline uranium-based compounds, while the interface and surface control can be a route to study the exotic electronic states in the strongly correlated systems.

## ACKNOWLEDGMENTS

This work was supported by the National Key Research and Development Program of China (Grant No. 2022YFA1402201) and the National Natural Science Foundation of China (Grants No. 11974319, No. 12122409, and No. 11904335).

## APPENDIX: EXPERIMENTS AND METHODS

*Sample preparation and STM measurements.* All the substrate preparations and depositions of uranium were performed in an ultrahigh vacuum (UHV) chamber with a base pressure better than  $8 \times 10^{-11}$  mbar. The single crystals of Cu (111) were prepared by cycles of Ar<sup>+</sup> sputtering and then annealed at 800 K for several minutes to obtain an atomically smooth and clean surface. Bulk U metal with a purity of 99.9% was heated to degas for a long time in the UHV chamber by an *e*-beam evaporator first, and then the U atoms were deposited onto the Cu (111) substrate. During the deposition process, the vacuum was better than  $2 \times 10^{-10}$  mbar. The growth rate of the UCu<sub>5</sub> (111) thin film was estimated to be about 1 u.c./h. All the STM measurements were carried out in another connected UHV chamber with a base pressure better than  $2 \times 10^{-11}$  mbar. The clean tungsten tips were used for STM measurements after annealing by the *e*-beam heater. All the  $dI/dV$  spectra were measured by a standard lock-in technique at the marked temperature.

- 
- [1] C. M. Varma, Mixed-valence compounds, *Rev. Mod. Phys.* **48**, 219 (1976).
  - [2] G. R. Stewart, Heavy-fermion systems, *Rev. Mod. Phys.* **56**, 755 (1984).
  - [3] C. Pfleiderer, Superconducting phases of *f*-electron compounds, *Rev. Mod. Phys.* **81**, 1551 (2009).
  - [4] Q. Si, Quantum criticality and global phase diagram of magnetic heavy fermions, *Phys. Status Solidi B* **247**, 476 (2010).
  - [5] O. Stockert, S. Kirchner, F. Steglich, and Q. Si, Superconductivity in Ce- and U-based “122” heavy-fermion compounds, *J. Phys. Soc. Jpn.* **81**, 011001 (2012).
  - [6] Q. M. Si and F. Steglich, Heavy fermions and quantum phase transitions, *Science* **329**, 1161 (2010).
  - [7] S.-i. Fujimori, Band structures of 4*f* and 5*f* materials studied by angle-resolved photoelectron spectroscopy, *J. Phys.: Condens. Matter* **28**, 153002 (2016).
  - [8] Y. Haga, H. Sakai, and S. Kambe, Recent advances in the 5*f*-relevant electronic states and unconventional superconductivity of actinide compounds, *J. Phys. Soc. Jpn.* **76**, 051012 (2007).
  - [9] Y. Onuki, R. Settai, K. Sugiyama, T. Takeuchi, T. C. Kobayashi, Y. Haga, and E. Yamamoto, Recent advances in the magnetism and superconductivity of heavy fermion systems, *J. Phys. Soc. Jpn.* **73**, 769 (2004).
  - [10] Q. Y. Chen, C. H. P. Wen, Q. Yao, K. Huang, Z. F. Ding, L. Shu, X. H. Niu, Y. Zhang, X. C. Lai, Y. B. Huang, G. B. Zhang, S. Kirchner, and D. L. Feng, Tracing crystal-field splittings in the rare-earth-based intermetallic CeIrIn<sub>5</sub>, *Phys. Rev. B* **97**, 075149 (2018).
  - [11] T. Willers, Z. Hu, N. Hollmann, P. O. Koerner, J. Gegner, T. Burmus, H. Fujiwara, A. Tanaka, D. Schmitz, H. H. Hsieh, H. J. Lin, C. T. Chen, E. D. Bauer, J. L. Sarrao, E. Goremychkin, M. Koza, L. H. Tjeng, and A. Severing, Crystal-field and Kondo-scale investigations of CeMIn<sub>5</sub> (*M* = Co, Ir, and Rh): A combined x-ray absorption and inelastic neutron scattering study, *Phys. Rev. B* **81**, 195114 (2010).
  - [12] A. Misiuk, J. Mulak, and A. Czopnik, Magnetic properties of uranium-compounds of low uranium contents-UCu<sub>5</sub>, U<sub>2</sub>Zn<sub>17</sub> and UCd<sub>11</sub>, *Bull. Acad. Pol. Sci., Ser. Sci. Chim.* **21**, 487 (1973).

- [13] A. Murasik, S. Ligenza, and A. Zygmunt, Magnetic-structure of  $\text{UCu}_5$ , *Phys. Status Solidi A* **23**, K163 (1974).
- [14] M. B. Brodsky and N. J. Bridger, Magnetic properties of  $\text{UCu}_5$  and  $\text{UNi}_5$ , in *Proceedings of the 19th Annual Conference on Magnetism and Magnetic Materials, Boston, MA*, AIP Conf. Proc. No. 18 (AIP, Melville, NY, 1973), pp. 357–361.
- [15] H. R. Ott, H. Rudigier, E. Felder, Z. Fisk, and B. Batlogg, Low-temperature state of  $\text{UCu}_5$ : Formation of heavy electrons in a magnetically ordered material, *Phys. Rev. Lett.* **55**, 1595 (1985).
- [16] A. Schenck, P. Birrer, F. N. Gyax, B. Hitti, E. Lippelt, M. Weber, P. Boni, P. Fischer, H. R. Ott, and Z. Fisk, Study of the 1-K phase transition in the heavy-electron compound  $\text{UCu}_5$  by muon spin resonance and neutron scattering, *Phys. Rev. Lett.* **65**, 2454 (1990).
- [17] N. Metoki, T. Osakabe, Y. Morii, Y. Onuki, and M. Date, Neutron-scattering study of the 1 K transition in a heavy-fermion system  $\text{UCu}_5$ , *J. Phys. Soc. Jpn.* **64**, 4491 (1995).
- [18] M. A. L. Delatorre, K. A. McEwen, M. Ellerby, C. Haworth, and M. Springford, The low-temperature phase-diagram of  $\text{UCu}_5$  determined from magnetization and magnetoresistance measurements, *J. Phys.: Condens. Matter* **7**, 9235 (1995).
- [19] H. Nakamura, Y. Kitaoka, M. Inoue, K. Asayama, and Y. Onuki, Magnetic-structure of antiferromagnetic heavy fermion  $\text{UCu}_5$ , *J. Magn. Magn. Mater.* **90–91**, 459 (1990).
- [20] H. Nakamura, Y. Kitaoka, K. Asayama, and Y. Onuki, Origin of the 1K-transition of  $\text{UCu}_5$ , *Phys. B (Amsterdam)* **171**, 329 (1991).
- [21] H. Nakamura, Y. Kitaoka, K. Asayama, Y. Onuki, and M. Shiga, Nuclear magnetic resonance in the antiferromagnetic heavy-fermion system  $\text{UCu}_5$ : Spin reorientation at 1 K, *J. Phys.: Condens. Matter* **6**, 10567 (1994).
- [22] B. Andraka, J. Dapprich, M. Baldus, P. Kumar, and G. R. Stewart, Magnetic-field investigation of the 1-K transition in  $\text{UCu}_5$ , *Phys. Rev. B* **45**, 7481 (1992).
- [23] A. Yamagishi, K. Senda, K. Kindo, M. Date, and Y. Onuki, Multistep magnetization of  $\text{UCu}_5$ , *J. Magn. Magn. Mater.* **108**, 211 (1992).
- [24] B. G. Ueland, C. F. Miclea, Y. Kato, O. Ayala-Valenzuela, R. D. McDonald, R. Okazaki, P. H. Tobash, M. A. Torrez, F. Ronning, R. Movshovich, Z. Fisk, E. D. Bauer, I. Martin, and J. D. Thompson, Controllable chirality-induced geometrical Hall effect in a frustrated highly correlated metal, *Nat. Commun.* **3**, 1067 (2012).
- [25] L. Degiorgi, H. R. Ott, M. Dressel, G. Gruner, and Z. Fisk, Optical probing of the antiferromagnetic phase-transitions in the heavy-electron compounds  $\text{U}_2\text{Zn}_{17}$  and  $\text{UCu}_5$ , *Europhys. Lett.* **26**, 221 (1994).
- [26] L. Degiorgi, H. R. Ott, M. Dressel, G. Gruner, C. Geibel, F. Steglich, and Z. Fisk, Optical investigation of the antiferromagnetic phase transitions in heavy-electron compounds, *Phys. B (Amsterdam)* **206**, 441 (1995).
- [27] L. Degiorgi, S. Thieme, H. R. Ott, M. Dressel, G. Gruner, Y. Dalichaouch, M. B. Maple, Z. Fisk, C. Geibel, and F. Steglich, The electrodynamic response of heavy-electron materials with magnetic phase transitions, *Z. Phys. B* **102**, 367 (1997).
- [28] H. Grohs, H. Hochst, P. Steiner, S. Hufner, and K. H. J. Buschow, XPS study of U,  $\text{UNi}_5$ ,  $\text{UCu}_5$  and  $\text{UNi}_{0.5}\text{Cu}_{4.5}$ , *Solid State Commun.* **33**, 573 (1980).
- [29] W.-D. Schneider, B. Reihl, N. Mårtensson, and A. J. Arko, Resonant photoemission study of  $\text{UNi}_{5-x}\text{Cu}_x$ , *Phys. Rev. B* **26**, 423 (1982).
- [30] *Cu-U binary phase diagram 0–100 at.% U: Datasheet from “PAULING FILE Multinaries Edition–2022” in Springer Materials*, edited by P. Villars and H. Okamoto (Springer-Verlag, Berlin, Heidelberg, 2022), and Material Phases Data System (MPDS), Switzerland, and National Institute for Materials Science (NIMS), Japan.
- [31] W. Feng, Q. Hao, Q. Chen, R. Qiu, X. Lai, J. Chen, and Q. Liu, Comparative study of adsorptions, reactions and electronic properties of U atoms on Cu(111), Ag(111), Au(111) and Ru(0001) surfaces, *Nanotechnology* **32**, 425704 (2021).
- [32] W. Feng, D. H. Xie, X. B. Luo, S. Y. Tan, Y. Liu, Q. Liu, Q. Hao, X. G. Zhu, Q. Zhang, Y. Zhang, Q. Y. Chen, and X. C. Lai, Crossover behavior of the localized to itinerant transition of 5f electrons in the antiferromagnetic Kondo lattice  $\text{USb}_2$ , *Phys. Rev. B* **104**, 235103 (2021).
- [33] P. Aynajian, E. H. da Silva Neto, A. Gyenis, R. E. Baumbach, J. D. Thompson, Z. Fisk, E. D. Bauer, and A. Yazdani, Visualizing heavy fermions emerging in a quantum critical Kondo lattice, *Nature (London)* **486**, 201 (2012).
- [34] P. Aynajian, E. H. D. Neto, C. V. Parker, Y. K. Huang, A. Pasupathy, J. Mydosh, and A. Yazdani, Visualizing the formation of the Kondo lattice and the hidden order in  $\text{URu}_2\text{Si}_2$ , *Proc. Natl. Acad. Sci. USA* **107**, 10383 (2010).
- [35] S. Ernst, S. Kirchner, C. Krellner, C. Geibel, G. Zwircknagl, F. Steglich, and S. Wirth, Emerging local Kondo screening and spatial coherence in the heavy-fermion metal  $\text{YbRh}_2\text{Si}_2$ , *Nature (London)* **474**, 362 (2011).
- [36] A. R. Schmidt, M. H. Hamidian, P. Wahl, F. Meier, A. V. Balatsky, J. D. Garrett, T. J. Williams, G. M. Luke, and J. C. Davis, Imaging the Fano lattice to ‘hidden order’ transition in  $\text{URu}_2\text{Si}_2$ , *Nature (London)* **465**, 570 (2010).
- [37] W. Zhang, W. Feng, X. Luo, S. Tan, D. Xie, Y. Liu, Y. Zhang, Q. Hao, Q. Zhang, X. Zhu, Q. Liu, Q. Chen, and X. Lai, Direct observation of the hybridization gap in both the hidden order and large moment antiferromagnetic phases in  $\text{URu}_2\text{Si}_2$ , *Phys. Rev. B* **106**, 165109 (2022).
- [38] V. Madhavan, W. Chen, T. Jamneala, M. F. Crommie, and N. S. Wingreen, Tunneling into a single magnetic atom: Spectroscopic evidence of the Kondo resonance, *Science* **280**, 567 (1998).
- [39] U. Fano, Effects of configuration interaction on intensities and phase shifts, *Phys. Rev.* **124**, 1866 (1961).
- [40] W. Feng, Q. Liu, C. Zhou, X. Lai, B. Li, and A. Zhao, Preserved Kondo effect of small cobalt atomic chains on Ru(0001) surface, *New J. Phys.* **18**, 123011 (2016).
- [41] V. Madhavan, W. Chen, T. Jamneala, M. F. Crommie, and N. S. Wingreen, Local spectroscopy of a Kondo impurity: Co on Au(111), *Phys. Rev. B* **64**, 165412 (2001).